Check for updates

How to cite: *Angew. Chem. Int. Ed.* **2021**, *60*, 21918–21926
International Edition: doi.org/10.1002/anie.202108010
German Edition: doi.org/10.1002/ange.202108010

Luminescence

Brightening up Circularly Polarized Luminescence of Monosubstituted Polyacetylene by Conformation Control: Mechanism, Switching, and Sensing

Sheng Wang[+], Deping Hu[+], Xiaoyan Guan, Siliang Cai, Ge Shi, Zhigang Shuai, Jie Zhang, Qian Peng,* and Xinhua Wan**

Abstract: *The first example of luminescent monosubstituted polyacetylenes (mono-PAs) is presented, based on a contracted cis-cisoid polyene backbone. It has an excellent circularly polarized luminescence (CPL) performance with a high dissymmetric factor (up to the order of 10^{-1}). The luminescence stems from the helical cis-cisoid PA backbone, which is tightly fixed by the strong intramolecular hydrogen bonds, thereby reversing the energy order of excited states and enabling an emissive energy dissipation. CPL switches are facilely achieved by the solvent and temperature through reversible conformational transition. By taking advantages of fast response and high sensitivity, the thin film of mono-PAs could be used as a CPL-based probe for quantitative detection of trifluoroacetic acid with a wider linear dynamic range than those of photoluminescence and circular dichroism. This work opens a new avenue to develop novel smart CPL materials through modulating conformational transition.*

Introduction

Circularly polarized luminescence (CPL), which indicates the molecular chirality in the excited state, is attracting enormous attention owing to its extensive applications in 3D displays, information technologies, photoelectric devices, biosensors, etc.[1] Compared to circular dichroism (CD) or nonpolarized photoluminescence (PL), CPL spectroscopy could eliminate the interferences of other achiral luminophores and chromophores, thereby displays higher sensitivity and resolution when applied in molecular sensors or detectors.[2] Responsive CPL materials under external stimuli, such as light,[3] pH,[4] metal ions,[2b,5] force,[6] etc.[7] have been achieved. However, it still remains a formidable challenge for the use of a CPL-based ratiometric probe for quantitative detection, which commonly requires regularly linear dynamic ranges of g_{lum} value, high g_{lum} value, and good switchability.[2a,8] Most of responsive CPL probes reported so far only present the relatively lower g_{lum} (mainly located between 10^{-5} and 10^{-2}), and limited linear relationship between g_{lum} and the analyte concentration, far away from the practical requirements. Examples of CPL probes satisfying all of the above features are even scarce.

Conjugated polymers, which commonly possess easy manufacturing processes, facile structural modification, and finely tunable emission wavelengths, have become one of promising CPL sensing materials.[9] Polyacetylene (PA) is an important archetypal conjugated polymer with unique photoelectric properties.[10] Optically active monosubstituted PAs (mono-PAs) are one type of the dynamic helical polymers featuring a highly stereoregular conjugated backbone, easily tunable helical conformations under external stimuli, and mild polymerization condition.[11] These characteristics make them promising candidates for stimuli-responsive CPL materials. However, mono-PAs are generally considered to be nonemissive due to the unfavorable energy levels of the ground and low-lying excited states ($E(1B_u) > E(2A_g)$, Figure 1a).[12] The $1B_u$ state decays into the $2A_g$ state via fast internal conversion, but the $2A_g$ to $1A_g$ transition is electronically dipole-forbidden according to symmetry selection rule.[12a] In comparison, the steric effect on the polyene backbone of disubstituted PAs (di-PAs) makes the energy level of the $1B_u$ state become lower than that of the $2A_g$ state, enabling an emissive energy dissipation from $1B_u$ to $1A_g$ state with electronically dipole-allowed transition.[13] But di-PAs cannot be applied as stimuli-responsive CPL materials due to their stable *trans-transoid* (*tt*) structure. Given the fact that most reported mono-PAs take stretched *cis-transoid* (*ct*) conformations,[14] we assume that the mono-PAs taking contracted *cis-cisoid* (*cc*) helical conformations possess the tight polyene backbone, in which the molecular motions would be restricted, thereby reversing the energy levels of $1B_u$ and $2A_g$, similar to the steric effect in di-PAs. We expect that optically active mono-PAs taking contracted *cc* helical con-

[*] Dr. S. Wang,[+] Dr. X. Guan, S. Cai, Dr. G. Shi, Prof. J. Zhang, Prof. X. Wan
Beijing National Laboratory for Molecular Sciences, Key Laboratory of Polymer Chemistry and Physics of Ministry of Education
College of Chemistry and Molecular Engineering
Peking University, Beijing 100871 (China)
E-mail: jz10@pku.edu.cn
xhwan@pku.edu.cn
Dr. D. Hu,[+] Prof. Z. Shuai
Key Laboratory of Organic OptoElectronics and Molecular Engineering of Ministry of Education, Department of Chemistry
Tsinghua University, Beijing 100084 (China)
Prof. Q. Peng
School of Chemical Sciences
University of Chinese Academy of Sciences
Beijing 100049 (China)
E-mail: qpeng@iccas.ac.cn
[+] These authors contributed equally to this work.
Supporting information and the ORCID identification number(s) for the author(s) of this article can be found under: https://doi.org/10.1002/anie.202108010.

 © 2021 Wiley-VCH GmbH

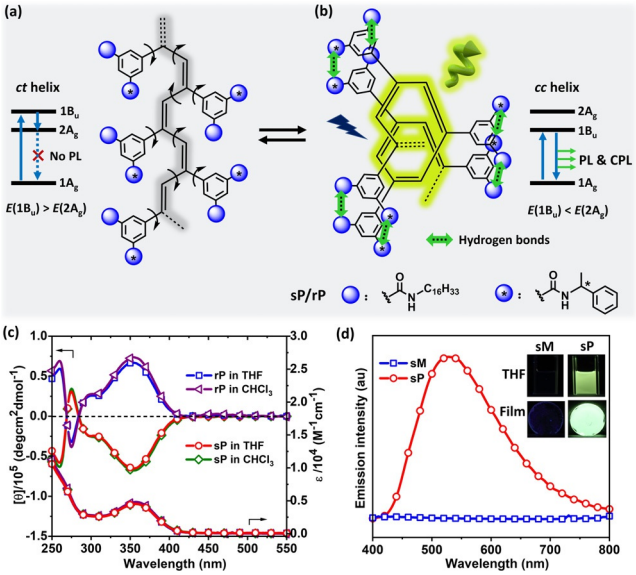

Figure 1. Molecular design to obtain fluorescent mono-PA. a),b) Strategy to obtain switchable fluorescence in mono-PA in our work and the energy levels of ground and low-lying excited states of *ct* helix (a) and *cc* helix (b). The contracted *cc* helix is stabilized by strong intramolecular hydrogen bonding. c) UV/Vis absorption and CD spectra of **sP** and **rP** in THF and $CHCl_3$. d) Emission spectra of **sM** and **sP** in THF (5.0×10^{-5} M). Excitation wavelength: 365 nm. Insert: Photographs of **sM** and **sP** in dilute THF solution, and their drop-cast film taken under UV illumination (365 nm).

formations could be photoluminescent and CPL-active even if no fluorophore pendant is attached (Figure 1b).

Herein, we report the first example of luminescent mono-PAs based on contracted *cc* polyene backbone, subverting the traditional cognition that mono-PA is non-emissive. Our molecular design strategy is built on poly(3,5-diamide substituted phenylacetylene)s, where strong intramolecular hydrogen bindings between the vicinal amide groups stabilize the contracted *cc* helix and restrict the possible molecular motions (Figure 1b). Even without pendant fluorophore, these mono-PAs can emit strong greenish yellow fluorescence. Experiments combined with theoretical calculations verify that this luminescence stems from the tight *cc* PA backbone. By taking advantage of the solvent- and thermo-responsiveness of hydrogen bonds, reversible fluorescent and CPL switch is realized in solution. Their cholesteric films exhibit excellent CPL with g_{lum} values up to the order of 10^{-1}, and can be reversibly turned ON/OFF via vapor-responsive conformational switch.

Results and Discussion

The target polymers **sP** and **rP** were prepared from the corresponding diamide monomers **sM** and **rM** with high yields and large molar masses (Scheme S1 and Table S1), following our previously reported procedures.[15] **sP** and **rP** exhibit absorptions peaked at 355 nm in THF, ascribed to the π–π* transition of contracted *cc* polyene backbone (Figure 1c).[15,16] In the same wavelength region, strong mono-signate Cotton effects are observed with perfect mirror images, evincing the formation of preferred one-handed helices with opposite screw senses.[15]

In THF, **sP** presents a broad emission band with an emission maximum at 530 nm upon photoexcitation at 365 nm, whereas the corresponding monomer **sM** is non-luminescent (Figure 1d). Similar emission spectra are observed in $CHCl_3$, powders, or in drop-cast film (Figures S5–S9). The absolute PL quantum yields (ϕ) are about 7% and 4% in THF and $CHCl_3$, respectively, and reach around 12% in films. Moreover, their PLs decay single exponentially at 530 nm (Figures 2a and S10, and Table S2). PL lifetime (τ) in solution is ≈0.5 ns, nearly half of that in solids or film, similar to that of di-PAs.[13e] It has been known that hydrogen bond donating solvent CH_3OH can destroy the hydrogen bonds and trigger the *cc*-to-*ct* transition of **sP** in $CHCl_3$.[15] Expectedly, the fluorescence is gradually quenched and vanishes completely when 11 vol% CH_3OH is added (Figures 2b and S11). Moreover, the *cis-trans* isomerization of -C=C- caused by grinding[17] also makes the fluorescence disappear (Figures S12 and S13), indicating again the importance of *cc* polyene structure in this unprecedented fluorescence.

It is worth noting that the aggregation-enhanced emission (AEE) is also observed in this system. Addition of non-solvents ethyl acetate (EtOAc) (Figure 2c) or acetone (Figures S15–S18) results in the distinct intensification of emission. In THF/EtOAc (10/90, v/v), the intensity is about twice stronger than that in THF (ϕ = 14%). Decreasing temperature has a similar effect. As shown in Figure 2d, the PL intensity of **sP** in THF gradually increases upon cooling and reaches a maximum at −75 °C. This emission enhancement could be attributed to the increasing restriction of intramolecular motions caused by lowering temperature or adding nonsolvent. At elevated temperatures, the emission intensity is obviously reduced (Figure S20), ascribed to the accelerated molecular motions.

To investigate the origin of luminescence, PL spectra are traced at different excitation wavelengths. Similar profiles of emission spectra peaked at 530 nm are observed when excited at different wavelengths from 240 to 420 nm (Figure 2e). No excitation-dependent PL behavior occurs, probably ascribed to the highly ordered main-chain stereostructure of **sP**. The optimal excitation wavelength is 365 nm, consistent with the absorption of polyene backbone (Figure 2f). The achiral poly(3,5-diamide substituted phenylacetylene)s (**aP-2C12**) with *cc* conformation in THF (Figure S21) also display PL properties in both solution and solid states, certifying that the chiroptical activity of the side groups have no effect on the luminescence. For a better comparison, as the conjugated polyene backbone is changed to unconjugated polystyrene, **V-sP**, only very weak ultraviolet fluorescence is observed (Figure S22). It further substantiates that the polyene backbones in **sP** and **rP** contribute to this strong long-wavelength emission.

To gain a deeper insight into the emitting mechanism of *cc* mono-PA, theoretical calculations were performed to unveil the excited state characters (Figure 3 and Table S3) by using the OM2/MRCI[18] (orthogonalization model 2 and multi-reference configuration interaction) methods. To simplify the

 © 2021 Wiley-VCH GmbH

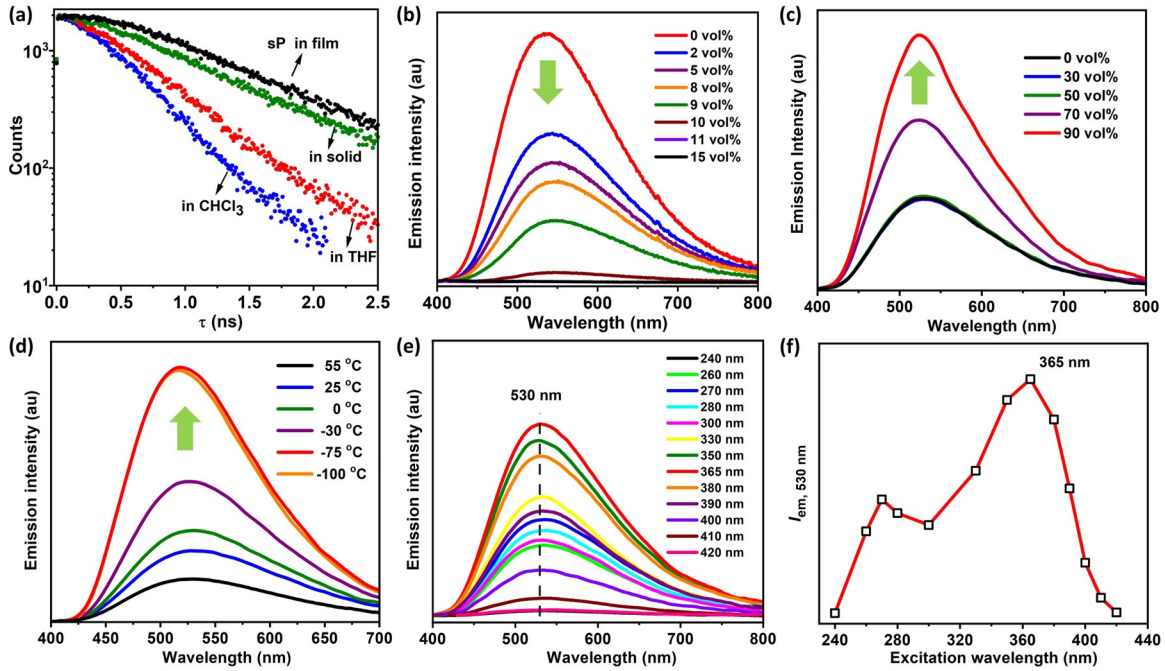

Figure 2. PL properties of mono-PA. a) PL decay of **sP** in $CHCl_3$, THF, solids, and drop-cast film at wavelength of 530 nm. Excitation wavelength: 378 nm. The film of **sP** was obtained from THF solutions (6.0 mg mL^{-1}). b) Emission spectra of **sP** in $CHCl_3$/CH_3OH mixtures with different vol% of CH_3OH and c) in THF/EtOAc mixtures with different vol% of EtOAc at 25 °C. d) Emission spectra of **sP** in THF at various temperatures. Excitation wavelength: 365 nm. e) Emission spectra of **sP** in THF at different excitation wavelengths. f) Relationship between emission intensity at 530 nm ($I_{em,\ 530\ nm}$) and the excitation wavelength. Concentration: 5.0×10^{-5} M.

calculation, only the PA backbone was kept in our model at first. The calculation results for *tt* PA were also presented for comparison. For S_1 minimum of *tt* PA, the S_1 is a dark state with a vanishing-oscillator strength, suggesting that no fluorescence can be observed after excitation according to Kasha rule (Figure 3a).[19] The S_1 mainly consists of one double excitation from HOMO to LUMO (34.1%), and two single excitations from HOMO-1 to LUMO (22.6%) and from HOMO to LUMO + 1 (23.5%) (Table S3). The HOMO and HOMO-1 are A_g symmetry, and the LUMO and LUMO + 1 belong to B_u symmetry. According to the principle of symmetry combination, S_1 is an A_g state. Since the ground state is still A_g one, the electric dipole transition from S_1 to S_0 is symmetry-forbidden. On the contrary, the main transition of S_2 is one single excitation from HOMO to LUMO, resulting in S_2 to be a B_u state. Thus, the electric dipole transition from S_2 to S_0 is symmetry-allowed. The excitation energy of the B_u state ($E(B_u)$) is largely decreased from 3.36 eV to 2.24 eV, when *tt* PA is changed to *cc* one. At this time, $E(A_g)$ slightly increases from 2.22 eV to 2.61 eV. Thus, the energy order of A_g and B_u is exchanged for *cc* PA and the S_1 becomes a bright state, which explains the fluorescence of *cc* conformer (Figure 3c,e). Moreover, the calculated results for S_1 minimum of *ct* PA are very close to that of *tt* PA (Figure 3b). The symmetry of S_1 and S_2 is A_g and B_u, respectively. Thus, the S_1 state is also a dark state with a very small oscillator strength (0.067), and no emission can be observed for *ct* conformer.

To understand the role of side chains in the emission of *cc* mono-PA, the model system was expanded and the phenyl substituted PA (PPA) was involved in our calculations (Figure 3d and Table S3). Comparing the results of PA with and without phenyl group, we can see that the excited state properties of these polymers are very close (Figure 3e). Both of the orbitals involved in the electronic transition for S_1 and S_2 are from the PA backbone. Therefore, we conclude that the side chains do not participate in the formation of excited state, even though they play an important role in stabilizing *cc* helix. In addition, the electronic characters do not change much from *ct* PA to *ct* PPA (Figure S23d), which further confirms our supposition.

Experimental results combined with theoretical calculations convince well that the emission behavior of *cc* poly(3,5-diamide substituted phenylacetylene)s originates from the tight polyene backbone, in which the molecular motions are terrifically restricted, thereby reversing the energy levels of $1B_u$ and $2A_g$ similar to the steric effect in di-PAs.[12a,13e] Considering some reported *cc* mono-PAs are non-luminescent,[15,16,20] it suggests that the *cc* structure is a necessary but insufficient prerequisite. Restriction is also indispensable to suppress the possible nonradiative channel thereby populating the radiative pathway. For those non-luminescent *cc* mono-PAs, their intramolecular interactions are presumably not strong enough to efficaciously restrict the molecular motions. By comparison, two amide substituents in our system can provide stronger intramolecular hydrogen bonds to fix the whole polyene backbone, and then brings out fluorescence. Aggregation and lowering temperature are beneficial to further enhance restriction and increase the PL efficiency. Moreover, it is worth noting that intense emission still can be excited under 270 nm, which correlates with the absorption of

 © 2021 Wiley-VCH GmbH

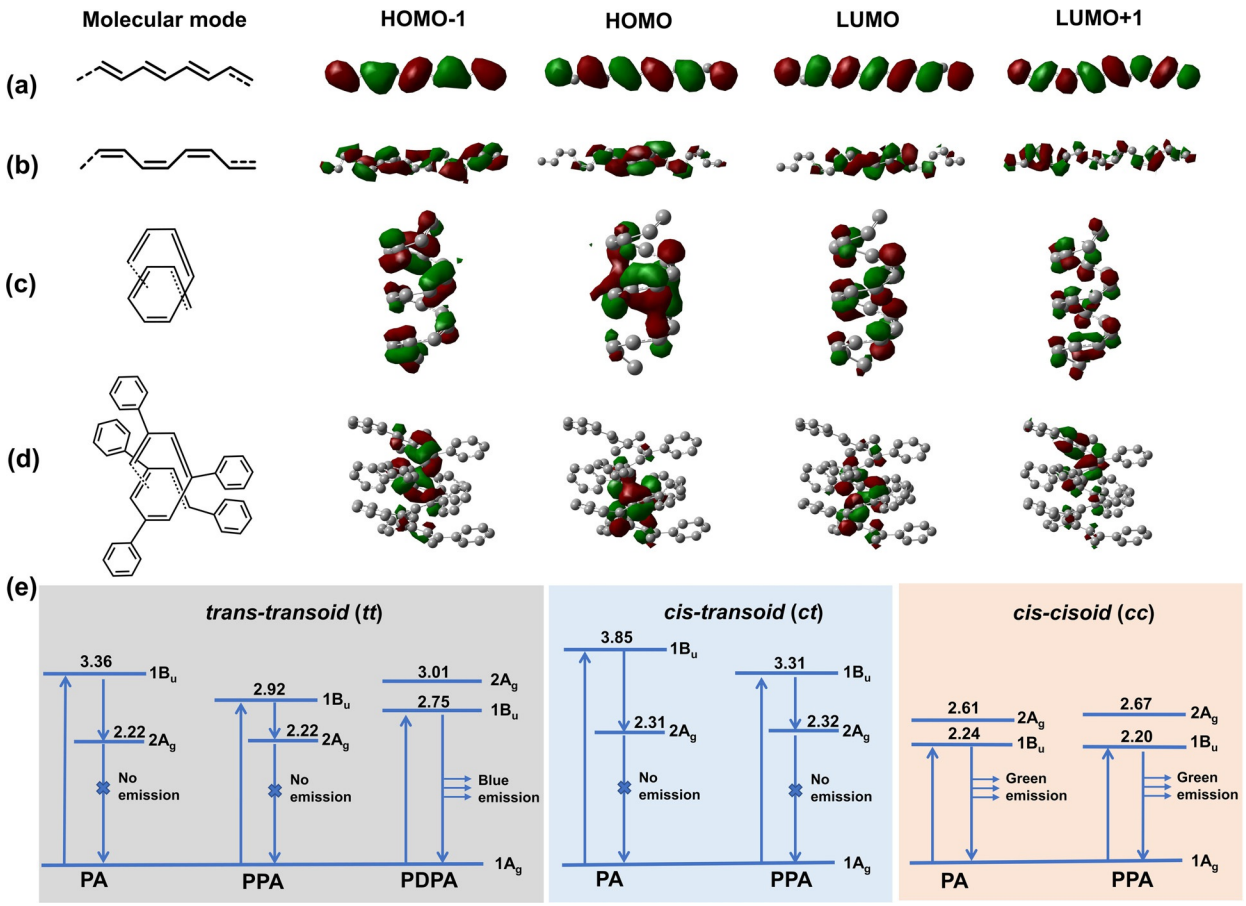

Figure 3. Theoretical calculations. a)–d) The partial molecular mode and frontier molecular orbitals of (a) *tt* PA, (b) *ct* PA, (c) *cc* PA, and (d) *cc* PPA of S_1 minima calculated using the OM2/MRCI method. The hydrogens are hidden for convenience. e) Energy levels of ground and low-lying excited states of *tt* PA, *tt* PPA, *tt* poly(di-phenylacetylene) (PDPA), *ct* PA, *ct* PPA, *cc* PA, and *cc* PPA. The unit of energy levels is eV.

pendant groups (Figure 2e,f). It suggests that adjacent phenyl pendants and amide groups are conjugated with polyene backbone, they can absorb the energy and transfer to the *cc* main chain, albeit with a lower PL efficiency.

The thermoresponsive helix–helix transition of **sP** can be achieved in the mixture of $CHCl_3$ and CH_3OH. In pure $CHCl_3$ or in a mixed solvent of $CHCl_3$ and CH_3OH containing less than 5 vol% CH_3OH ($V_{CH3OH} < 5$ vol%), **sP** retains *cc* helix in the temperature ranging from 2 to 30 °C (Figure S24). While at $V_{CH3OH} = 5$ vol%, reversible temperature-dependent conformational variation occurs. During the cooling process, the strong absorption centered at 355 nm gradually decreases accompanied with the appearance of intense absorption at 455 nm, which is ascribed to the stretched *ct* polyene backbone (Figure 4a). Meanwhile, the negative Cotton effects of *cc* main chain at 355 nm vanish, and a weak positive one appears at around 455 nm accordingly, consistent with the *cc*-to-*ct* transition.[15,16] The transition completes at 15 °C, and an inverse process can be triggered upon heating (Figure S25). This behavior can be rationalized by the competition of intramolecular hydrogen bonding and intermolecular hydrogen bonding between the polymer and hydrogen bond donating solvent, that is, $CHCl_3$. At high temperature, intramolecular hydrogen bonding is stronger than the hydrogen bonding between the polymer and solvents and favors the existence of *cc* helix. Whereas the latter becomes dominant at a lower temperature since the solvent molecules interact more strongly with the macromolecules, which trigger *cc*-to-*ct* transition. Interestingly, the transition temperature can be tuned by altering CH_3OH content. Increasing the volume fraction of CH_3OH raises the critical temperature (T_{ct}) at which *cc* helix completely transfers to the *ct* one (Figures S26 and S27). In the case of $V_{CH3OH} = 8$ vol% and 15 vol%, T_{ct} increases to 22 and 33 °C (Figure 4d), respectively. As the hydrogen bond donating ability of CH_3OH is stronger than $CHCl_3$, its addition can result in the formation of more defects, such like helical reversals, which increases the flexibility of polymer chains. So higher temperature is needed to extrude out solvent molecules and reconstruct intramolecular hydrogen bonding. According to the inverse Arrhenius rate equation: $\tau^* = \tau_0 \exp(E_a/RT)$ (Figures 4f and S32), activation energy (E_a) is estimated to be 76.3, 121.5, and 147.3 kJ mol^{-1}, respectively, for $V_{CH3OH} = 5$, 8, and 15 vol%. E_a increases with V_{CH3OH}, indicating an increased conformational transition barrier with increasing V_{CH3OH}. Similar conclusions can be obtained from PL spectra. The fluorescence gradually vanishes with temperature decreasing, and slowly recovers to the initial spectrum again during the heating process in agreement with the conformational changes (Figures 4b and S28–S30). This *cc*-to-*ct* transition

 © 2021 Wiley-VCH GmbH

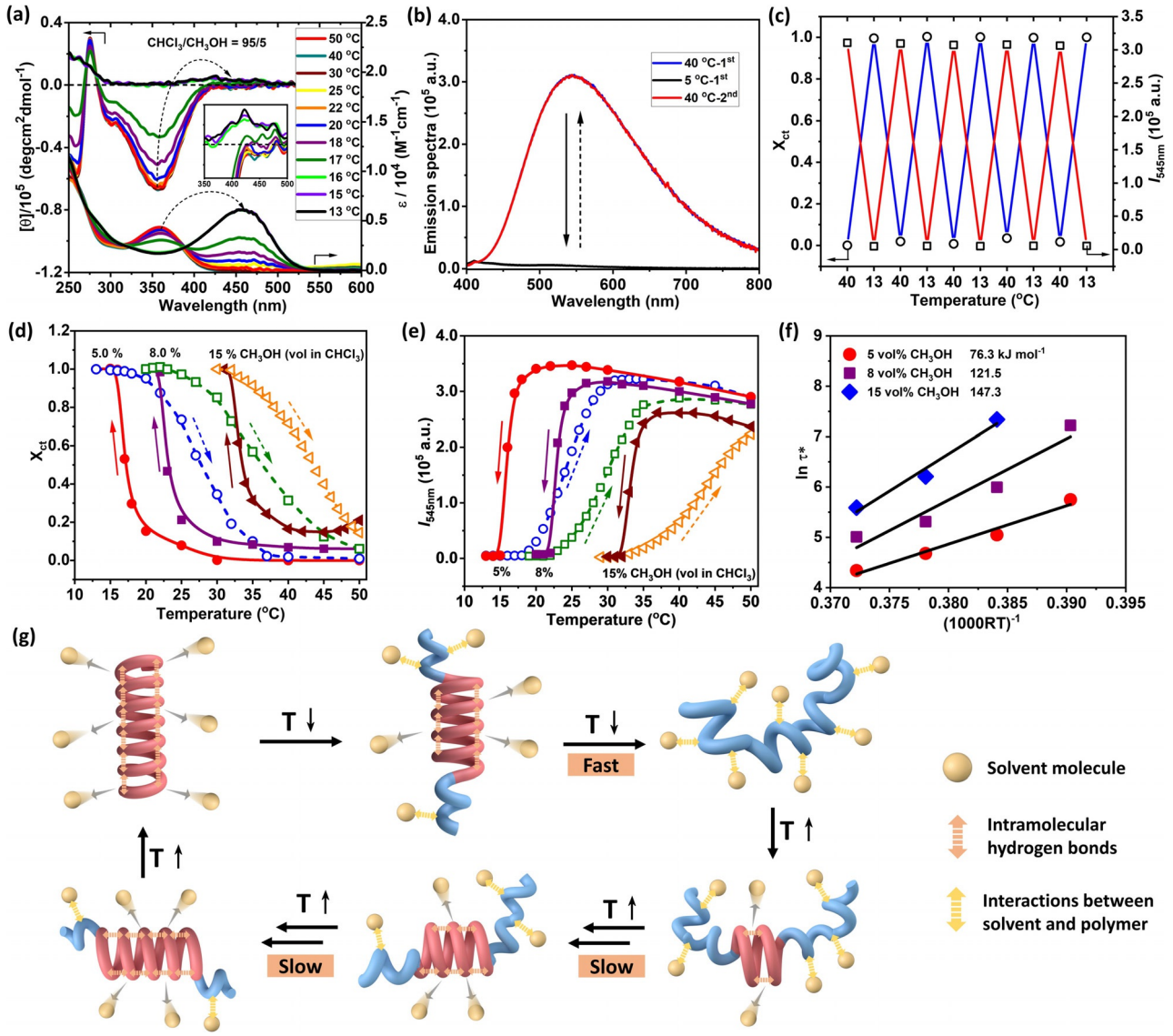

Figure 4. Thermoresponsive conformation and fluorescent switch. a) UV/Vis and CD spectra of **sP** in $CHCl_3/CH_3OH$ (v/v, 95/5) mixtures during cooling process. Inset: The partial amplification of CD spectra from 350 nm to 500 nm. b) Reversible PL spectra of **sP** in $CHCl_3/CH_3OH$ (v/v, 95/5) mixtures changing with temperature. c) X_{ct} ($X_{ct} = (\varepsilon_{abs} - \varepsilon_{cc})/(\varepsilon_{ct} - \varepsilon_{cc})$ is used to quantitatively evaluate the content of *ct* helix) and emission intensity at 545 nm (I_{545nm}) reversibly switch with alternative temperature change in $CHCl_3/CH_3OH$ (v/v, 95/5) mixtures. d) X_{ct} and e) I_{545nm} change with temperature during the cooling (solid line and closed symbol) and heating process (dash line and open symbol) in different solvent mixtures. f) Characteristic conformation transition time (τ*) exhibits an Arrhenius temperature dependence for different $CH_3OH/CHCl_3$ mixtures. Solid lines are fits to the inverse Arrhenius rate equation: $\tau^* = \tau_0 \exp(E_a/RT)$. g) Representation of conformational transition of **sP** during the cooling and heating processes.

and fluorescence change exhibit a good reversibility. The on/off switching of fluorescence was repeated up to five cycles without visible fatigue (Figures 4c and S31).

It is noteworthy that obvious hysteresis exists between the heating and cooling transition curves (Figure 4d,e). During the cooling process, once a small amount of intramolecular hydrogen bonds between amide groups are destroyed, *cc* conformer will quickly transfer to *ct* conformer (Figure 4g), showing a fast transition process. But for *ct* conformer, the polymer is surrounded by large amounts of solvent molecules and controlled by the intermolecular hydrogen bonding. Only most of the solvent molecules are extruded out at elevated temperature, can the partial *ct* polymer chain transfer to *cc* conformation. The reorganization process of intramolecular hydrogen bonding is stepwise and much slower than its destroying process, leading to the occurrence of hysteresis.

Because of the presence of both helicity and photoluminescence, CPL is expected for **sP** and **rP**. In THF, strong CPL signals are observed at ca. 530 nm (Figure 5a), which corresponds to the emission peak of the polyene backbone, and the g_{lum} values are +0.0037 and −0.0028 for **rP** and **sP** (Figure S33), respectively. Similar CPL performance is obtained in other solvents like $CHCl_3$, $CHCl_3/CH_3OH$ mixtures (Figure 5b), and *o*-dichlorobenzene (Figures S35, S36). It

 © 2021 Wiley-VCH GmbH

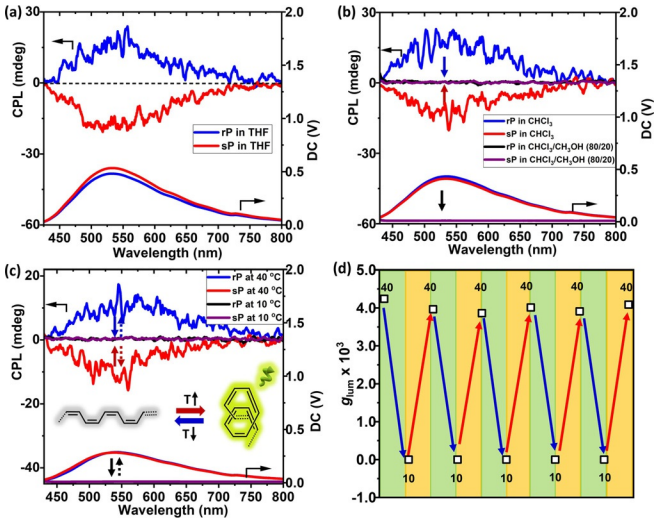

Figure 5. Stimuli-responsive CPL in solution. a),b) CPL spectra of **sP** and **rP** in THF (a), $CHCl_3$, and $CHCl_3/CH_3OH$ (80/20, v/v) (b) at 25 °C. c) CPL spectra of **sP** and **rP** in $CHCl_3/CH_3OH$ (95/5, v/v) at 10 and 40 °C. d) g_{lum} of **rP** in $CHCl_3/CH_3OH$ (95/5, v/v) switched by alternatively altering the temperature between 40 and 10 °C. $c = 0.5$ mM.

exhibits very good stimuli-responsive behavior via varying the solvent polarity and temperature. At high contents of CH_3OH (20 vol %), the strong CPL disappears (Figure 5b), coinciding with the *cc*-to-*ct* transition. Moreover, the above temperature-dependent conformational transition can be well applied to turn ON/OFF the CPL performance of **rP** and **sP**. With the temperature decreasing to 10 °C, the *cc* helix transfers to the *ct* one, accompanied with the disappearance of CPL (Figure 5c). Upon the temperature increasing to 40 °C, the initial CPL is recovered (Figure S37), which presents an outstanding reversibility without the apparent decline even after five cycles (Figure 5d). Brightness is another important parameter of CPL (B_{CPL}).[21] It is defined as $B_{CPL} = \varepsilon_\lambda \times \varphi \times |g_{lum}|/2$, where ε_λ and φ is the molar extinction coefficient measured at the excitation wavelength (λ) and the emission quantum yield, respectively. B_{CPL} in THF and $CHCl_3$ is evaluated as 0.62 $M^{-1}\cdot cm^{-1}$ and 0.36 $M^{-1}\cdot cm^{-1}$, respectively. In $CHCl_3/CH_3OH$ (95/5, v/v), B_{CPL} also presents the similar thermo-responsiveness (Figure S38).

Thanks to the large aspect ratio of contracted *cc* helices, both **sP** and **rP** are able to form cholesteric mesophases as evidenced by the fingerprint textures observed under polarizing optical microscope (Figures 6c and S43). The cholesteric films display remarkable complementary CPL signals centered at around the PL emission bands (Figure 6a). The g_{lum} values of **sP** and **rP** in films are +0.17 and −0.18, close to the largest value achieved in the di-PAs.[13e] No obvious optical anisotropy is observed in film (Figure S39). Moreover, their films exhibit the characteristic bisignate Cotton effects in CD spectra at the region of the absorption of polyene backbone (Figure 6b), further evincing the formation of chiral supramolecular structure.

The helical structure and CPL property of **sP** and **rP** in N*-LC film also can be reversibly switched ON/OFF with the acidic vapor. Upon exposure to trifluoroacetic acid (TFA) vapor, the color of N*-LC film quickly changed from light yellow to orange in 1 min, accompanied with the red shift of the absorption of polyene backbone from 360 nm to 450 nm

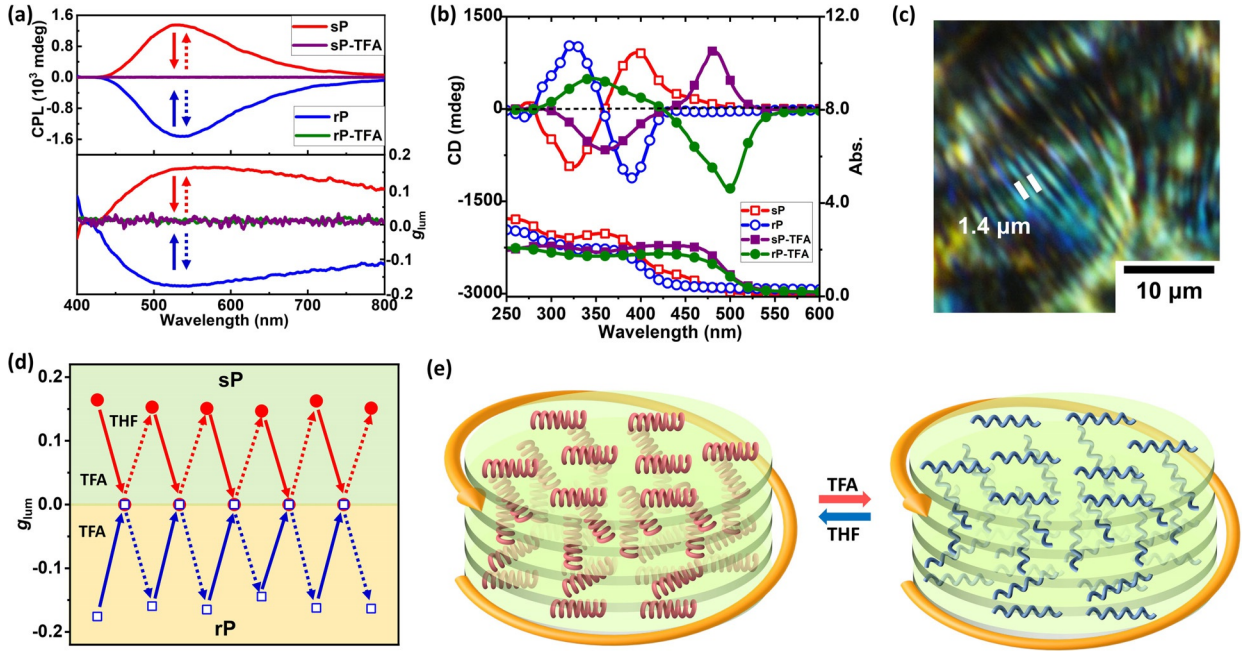

Figure 6. Stimuli-responsive CPL in N*-LC film. a),b) CPL, g_{lum} (a), UV/Vis, and CD (b) spectra of **sP**, **rP**, **sP-TFA**, and **rP-TFA** in drop-cast N*-LC film before and after treatment of TFA vapor for 1 min. The measurements were carried out with excitation using unpolarized light at 365 nm. c) The partial amplification of POM image (Supporting Information, Figure S37) of **rP** in the drop-cast film showing a fingerprint texture with a half helical pitch of 1.4 μm. d) g_{lum} of **sP** and **rP** in in drop-cast N*-LC film switched by the alternative treatment of TFA and THF vapor. e) Representation of N*-LC phase and the conformational switch for **rP**. Red and blue helices represent *cc* and *ct* PPA backbones, respectively.

 © 2021 Wiley-VCH GmbH

(Figure 6b). The corresponding main-chain Cotton effects present the coincident shift, evincing the conformational transition from *cc* to *ct* helices. At this time, the fluorescence and CPL disappeared (Figure 6a). Considering the film of **rP-TFA** maintains the N*-LC texture (Figure S45), it suggests that TFA vapor just switches the helical conformation instead of its assembly structure (Figure 6e). When exposed to THF vapor for 48 h, the *cc* helix and CPL intensity is recovered (Figure S40). An alternative treatment with TFA and THF vapors can reversibly tune the CPL property. Its g_{lum} value does not show obvious fatigue even after five cycles (Figure 6d), exhibiting an excellent switching performance.

TFA has been widely used in the production of pharmaceuticals, pesticides, and dyes, and becomes one of the tricky industrial pollutant. Its detection is of great significance to the human health and environmental protection. Based on the fast response and high g_{lum} value, our CPL switch was then applied to quantitively detect TFA. Different amounts of TFA were dissolved in $CHCl_3$. The CPL intensity can quickly respond to TFA vapor even in the low fraction of 0.2 vol% of TFA in $CHCl_3$, showing a high sensitivity (Figure 7a). CPL intensity diminishes fast with the increasing content of TFA, and completely disappears at 1.0 vol% of TFA (Figure 7a,b). The g_{lum} value is linearly proportional to the content of TFA in the range of 0.2–1.0 vol% ($R^2 = 0.9994$), evincing the feasibility of quantitative detection. By contrast, CD and PL spectroscopy exhibit the relatively lower sensitivity, worse linear relationship, and narrower detection range (Figure 7b). The complicated CD spectral change with the TFA content seriously hinders its application in quantitatively detecting TFA (Figure S41), further indicating the unique superiority of CPL in molecular sensor. Moreover, for other common organic acid like formic acid (FA), acetic acid (AA), propionic acid (PA), and butyric acid (BA), they are unable to quench CPL at the same condition (1 vol% for 1 min, Figures 7c and S42), exhibiting an outstanding specific identification to TFA.

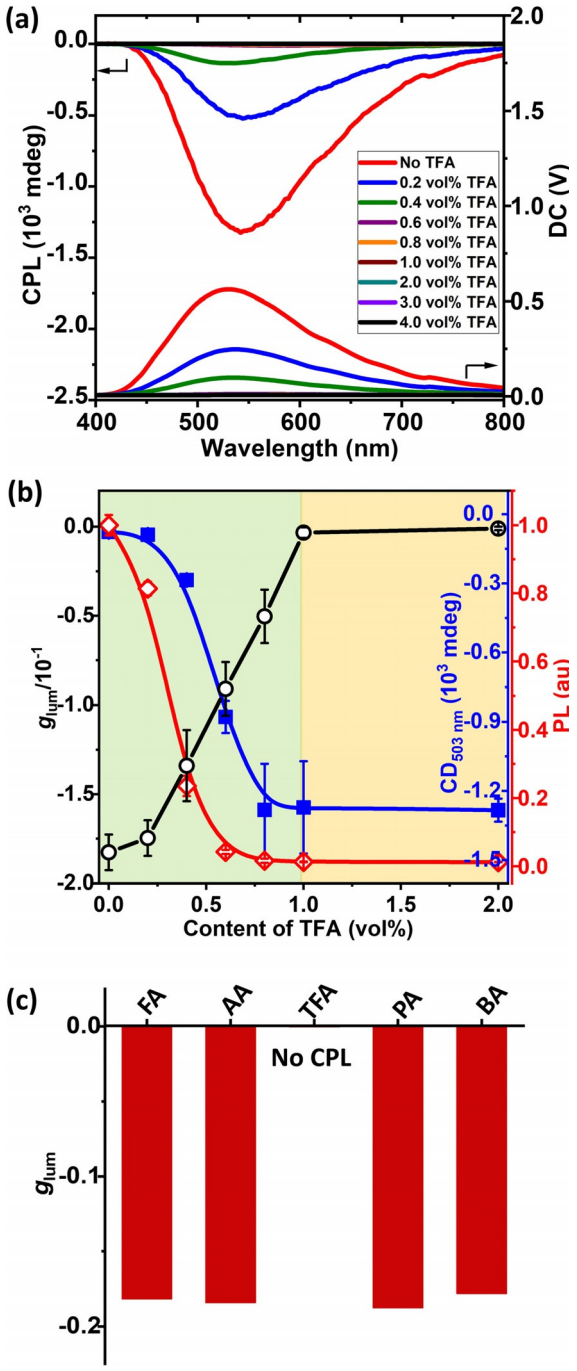

Figure 7. CPL sensor. a) CPL and DC spectra of **rP** in drop-cast N*-LC film changed with different TFA contents in $CHCl_3$. The responsive time to the mixed solvent vapor was set as 1 min. b) The quantitative relationship between CD intensity at 503 nm, PL intensity, g_{lum} and the TFA content in $CHCl_3$. c) g_{lum} of **rP** film after exposed to different organic acids (FA, AA, TFA, PA, and BA) in $CHCl_3$ (1 vol%) for 1 min.

Conclusion

We have demonstrated the first examples of circularly polarized luminescent mono-PAs bearing no pendant fluorophore. The key of molecular design is the introduction of two amide substituents at 3,5-positions of poly(phenylacetylene), which helps stabilize the contracted *cc* helix of polyene backbone through the intramolecular hydrogen bonding between the vicinal amide groups. Such a compacted macromolecular architecture not only exchanges the energy level order of A_g and B_u but also restricts intramolecular motions that usually suppress radiative energy dissipation, thereby enabling main-chain fluorescence. Reversible fluorescent switch can be on-demand achieved by changing temperature through *cc*-to-*ct* helical transition. The films cast from chiral nematic solutions exhibit excellent CPL property with g_{lum} values as large as 0.18. By taking advantage of the stimuli-responsive conformational transition, the CPL property can be used to specific identification and quantitative detection of TFA. Our work highlights the significance of conformational transition on exchanging the electronic energy level of polyene backbone, the concept of which may be appliable to other conjugated polymers and enriches molecular design toolkit for novel stimuli responsive CPL materials.

 © 2021 Wiley-VCH GmbH

Acknowledgements

The financial support from the National Natural Science Foundation of China (No. 51833001 and 52073001) is greatly appreciated.

Conflict of Interest

The authors declare no conflict of interest.

Keywords: circularly polarized luminescence · conformational transition · CPL sensor · polyacetylene · stimuli-responsiveness

[1] a) Y. Kim, B. Yeom, O. Arteaga, S. J. Yoo, S. G. Lee, J. G. Kim, N. A. Kotov, *Nat. Mater.* **2016**, *15*, 461 – 468; b) Y. Yang, R. C. da Costa, M. J. Fuchter, A. J. Campbell, *Nat. Photonics* **2013**, *7*, 634 – 638; c) D. M. Lee, J. W. Song, Y. J. Lee, C. J. Yu, J. H. Kim, *Adv. Mater.* **2017**, *29*, 1700907; d) E. Peeters, M. P. T. Christiaans, R. A. J. Janssen, H. F. M. Schoo, H. P. J. M. Dekkers, E. W. Meijer, *J. Am. Chem. Soc.* **1997**, *119*, 9909 – 9910; e) D. W. Zhang, M. Li, C. F. Chen, *Chem. Soc. Rev.* **2020**, *49*, 1331 – 1343; f) T. Zhao, J. Han, P. Duan, M. Liu, *Acc. Chem. Res.* **2020**, *53*, 1279 – 1292; g) M. C. Heffern, L. M. Matosziuk, T. J. Meade, *Chem. Rev.* **2014**, *114*, 4496 – 4539; h) R. Carr, N. H. Evans, D. Parker, *Chem. Soc. Rev.* **2012**, *41*, 7673 – 7686.

[2] a) Y. Sang, J. Han, T. Zhao, P. Duan, M. Liu, *Adv. Mater.* **2019**, e1900110; b) Y. Imai, Y. Nakano, T. Kawai, J. Yuasa, *Angew. Chem. Int. Ed.* **2018**, *57*, 8973 – 8978; *Angew. Chem.* **2018**, *130*, 9111 – 9116; c) P. Reiné, J. Justicia, S. P. Morcillo, S. Abbate, B. Vaz, M. Ribagorda, Á. Orte, L. Álvarez de Cienfuegos, G. Longhi, A. G. Campaña, D. Miguel, J. M. Cuerva, *J. Org. Chem.* **2018**, *83*, 4455 – 4463.

[3] a) H. Jiang, Y. Jiang, J. Han, L. Zhang, M. Liu, *Angew. Chem. Int. Ed.* **2019**, *58*, 785 – 790; *Angew. Chem.* **2019**, *131*, 795 – 800; b) J. Qiao, S. Lin, J. Li, J. Tian, J. Guo, *Chem. Commun.* **2019**, *55*, 14590 – 14593; c) Y. Hashimoto, T. Nakashima, D. Shimizu, T. Kawai, *Chem. Commun.* **2016**, *52*, 5171 – 5174.

[4] a) S. Tong, J. T. Li, D. D. Liang, Y. E. Zhang, Q. Y. Feng, X. Zhang, J. Zhu, M. X. Wang, *J. Am. Chem. Soc.* **2020**, *142*, 14432 – 14436; b) K. Takaishi, M. Yasui, T. Ema, *J. Am. Chem. Soc.* **2018**, *140*, 5334 – 5338; c) D. Niu, L. Ji, G. Ouyang, M. Liu, *ACS Appl. Mater. Interfaces* **2020**, *12*, 18148 – 18156.

[5] a) T. Zhao, J. Han, X. Jin, Y. Liu, M. Liu, P. Duan, *Angew. Chem. Int. Ed.* **2019**, *58*, 4978 – 4982; *Angew. Chem.* **2019**, *131*, 5032 – 5036; b) P. Reiné, A. M. Ortuño, S. Resa, L. Álvarez de Cienfuegos, V. Blanco, M. J. Ruedas-Rama, G. Mazzeo, S. Abbate, A. Lucotti, M. Tommasini, S. Guisán-Ceinos, M. Ribagorda, A. G. Campaña, A. Mota, G. Longhi, D. Miguel, J. M. Cuerva, *Chem. Commun.* **2018**, *54*, 13985 – 13988; c) A. Homberg, E. Brun, F. Zinna, S. Pascal, M. Górecki, L. Monnier, C. Besnard, G. Pescitelli, L. Di Bari, J. Lacour, *Chem. Sci.* **2018**, *9*, 7043 – 7052.

[6] S. Lee, K. Y. Kim, S. H. Jung, J. H. Lee, M. Yamada, R. Sethy, T. Kawai, J. H. Jung, *Angew. Chem. Int. Ed.* **2019**, *58*, 18878 – 18882; *Angew. Chem.* **2019**, *131*, 19054 – 19058.

[7] a) K. Takaishi, K. Iwachido, T. Ema, *J. Am. Chem. Soc.* **2020**, *142*, 1774 – 1779; b) X. Yang, M. Zhou, Y. Wang, P. Duan, *Adv. Mater.* **2020**, *32*, 2000820; c) Z. B. Sun, J. K. Liu, D. F. Yuan, Z. H. Zhao, X. Z. Zhu, D. H. Liu, Q. Peng, C. H. Zhao, *Angew. Chem. Int. Ed.* **2019**, *58*, 4840 – 4846; *Angew. Chem.* **2019**, *131*, 4894 – 4900; d) A. Gopal, M. Hifsudheen, S. Furumi, M. Takeuchi, A. Ajayaghosh, *Angew. Chem. Int. Ed.* **2012**, *51*, 10505 – 10509; *Angew. Chem.* **2012**, *124*, 10657 – 10661; e) Y. Chen, P. Lu, Z. Li, Y. Yuan, Q. Ye, H. Zhang, *ACS Appl. Mater. Interfaces* **2020**, *12*, 56604 – 56614; f) K. Dhbaibi, L. Favereau, M. Srebro-Hooper, C. Quinton, N. Vanthuyne, L. Arrico, T. Roisnel, B. Jamoussi, C. Poriel, C. Cabanetos, J. Autschbach, J. Crassous, *Chem. Sci.* **2020**, *11*, 567 – 576; g) Y. Wu, L. H. You, Z.-Q. Yu, J.-H. Wang, Z. Meng, Y. Liu, X.-S. Li, K. Fu, X.-K. Ren, B. Z. Tang, *ACS Mater. Lett.* **2020**, *2*, 505 – 510.

[8] a) W. J. Li, Q. Gu, X. Q. Wang, D. Y. Zhang, Y. T. Wang, X. He, W. Wang, H. B. Yang, *Angew. Chem. Int. Ed.* **2021**, *60*, 9507 – 9515; *Angew. Chem.* **2021**, *133*, 9593 – 9601; b) H. Maeda, Y. Bando, K. Shimomura, I. Yamada, M. Naito, K. Nobusawa, H. Tsumatori, T. Kawai, *J. Am. Chem. Soc.* **2011**, *133*, 9266 – 9269.

[9] a) K. Watanabe, H. Iida, K. Akagi, *Adv. Mater.* **2012**, *24*, 6451 – 6456; b) A. Satrijo, S. C. J. Meskers, T. M. Swager, *J. Am. Chem. Soc.* **2006**, *128*, 9030 – 9031; c) D. Lee, Y.-J. Jin, H. Kim, N. Suzuki, M. Fujiki, T. Sakaguchi, S. K. Kim, W.-E. Lee, G. Kwak, *Macromolecules* **2012**, *45*, 5379 – 5386; d) Y. Wang, Y. Li, S. Liu, F. Li, C. Zhu, S. Li, Y. Cheng, *Macromolecules* **2016**, *49*, 5444 – 5451; e) C. Kulkarni, M. H. C. van Son, D. Di Nuzzo, S. C. J. Meskers, A. R. A. Palmans, E. W. Meijer, *Chem. Mater.* **2019**, *31*, 6633 – 6641; f) L. Xu, C. Wang, Y. X. Li, X. H. Xu, L. Zhou, N. Liu, Z. Q. Wu, *Angew. Chem. Int. Ed.* **2020**, *59*, 16675 – 16682; *Angew. Chem.* **2020**, *132*, 16818 – 16825; g) W. Zheng, T. Ikai, E. Yashima, *Angew. Chem. Int. Ed.* **2021**, *60*, 11294 – 11299; *Angew. Chem.* **2021**, *133*, 11394 – 11399.

[10] a) H. Shirakawa, *Angew. Chem. Int. Ed.* **2001**, *40*, 2574 – 2580; *Angew. Chem.* **2001**, *113*, 2642 – 2648; b) A. J. Heeger, *Angew. Chem. Int. Ed.* **2001**, *40*, 2591 – 2611; *Angew. Chem.* **2001**, *113*, 2660 – 2682; c) A. G. MacDiarmid, *Angew. Chem. Int. Ed.* **2001**, *40*, 2581 – 2590; *Angew. Chem.* **2001**, *113*, 2649 – 2659; d) K. Akagi, *Chem. Rev.* **2009**, *109*, 5354 – 5401.

[11] a) E. Yashima, N. Ousaka, D. Taura, K. Shimomura, T. Ikai, K. Maeda, *Chem. Rev.* **2016**, *116*, 13752 – 13990; b) F. Freire, E. Quiñoá, R. Riguera, *Chem. Rev.* **2016**, *116*, 1242 – 1271; c) J. W. Y. Lam, B. Z. Tang, *Acc. Chem. Res.* **2005**, *38*, 745 – 754.

[12] a) B. A. San Jose, K. Akagi, *Polym. Chem.* **2013**, *4*, 5144 – 5161; b) B. A. San Jose, S. Matsushita, Y. Moroishi, K. Akagi, *Macromolecules* **2011**, *44*, 6288 – 6302; c) B. Zhao, H. Yu, K. Pan, Z. Tan, J. Deng, *ACS Nano* **2020**, *14*, 3208 – 3218.

[13] a) R. Hidayat, S. Tatsuhara, D. W. Kim, M. Ozaki, K. Yoshino, M. Teraguchi, T. Masuda, *Phys. Rev. B* **2000**, *61*, 10167 – 10173; b) Z. G. Soos, S. Ramasesha, D. S. Galvão, *Phys. Rev. Lett.* **1993**, *71*, 1609 – 1612; c) Z. Shuai, J. L. Brédas, S. K. Pati, S. Ramasesha, *Phys. Rev. B* **1997**, *56*, 9298 – 9301; d) X. Wang, J. Z. Sun, B. Z. Tang, *Prog. Polym. Sci.* **2018**, *79*, 98 – 120; e) B. A. San Jose, S. Matsushita, K. Akagi, *J. Am. Chem. Soc.* **2012**, *134*, 19795 – 19807; f) B. A. San Jose, J. Yan, K. Akagi, *Angew. Chem. Int. Ed.* **2014**, *53*, 10641 – 10644; *Angew. Chem.* **2014**, *126*, 10817 – 10820; g) W. E. Lee, Y. J. Jin, L. S. Park, G. Kwak, *Adv. Mater.* **2012**, *24*, 5604 – 5609; h) Y.-J. Jin, J.-E. Bae, K.-S. Cho, W.-E. Lee, D.-Y. Hwang, G. Kwak, *Adv. Funct. Mater.* **2014**, *24*, 1928 – 1937; i) K. Maeda, M. Nozaki, K. Hashimoto, K. Shimomura, D. Hirose, T. Nishimura, G. Watanabe, E. Yashima, *J. Am. Chem. Soc.* **2020**, *142*, 7668 – 7682; j) H. Kim, K.-U. Seo, Y.-J. Jin, C.-L. Lee, M. Teraguchi, T. Kaneko, T. Aoki, G. Kwak, *ACS Macro Lett.* **2016**, *5*, 622 – 625.

[14] a) K. Shimomura, T. Ikai, S. Kanoh, E. Yashima, K. Maeda, *Nat. Chem.* **2014**, *6*, 429 – 434; b) K. Maeda, H. Mochizuki, M. Watanabe, E. Yashima, *J. Am. Chem. Soc.* **2006**, *128*, 7639 – 7650; c) K. K. L. Cheuk, B. S. Li, J. W. Y. Lam, Y. Xie, B. Z. Tang, *Macromolecules* **2008**, *41*, 5997 – 6005; d) S. Arias, F. Freire, M. Calderón, J. Bergueiro, *Angew. Chem. Int. Ed.* **2017**, *56*, 11420 – 11425; *Angew. Chem.* **2017**, *129*, 11578 – 11583; e) S. Wang, X. Feng, J. Zhang, X. Wan, *Chin. J. Chem.* **2020**, *38*, 570 – 576.

[15] S. Wang, J. Chen, X. Feng, G. Shi, J. Zhang, X. Wan, *Macromolecules* **2017**, *50*, 4610 – 4615.

 © 2021 Wiley-VCH GmbH

[16] a) S. Wang, X. Feng, J. Zhang, P. Yu, Z. Guo, Z. Li, X. Wan, *Macromolecules* **2017**, *50*, 3489 – 3499; b) S. Wang, G. Shi, X. Guan, J. Zhang, X. Wan, *Macromolecules* **2018**, *51*, 1251 – 1259; c) S. Wang, X. Feng, Z. Zhao, J. Zhang, X. Wan, *Macromolecules* **2016**, *49*, 8407 – 8417.

[17] a) K. Maeda, S. Wakasone, K. Shimomura, T. Ikai, S. Kanoh, *Macromolecules* **2014**, *47*, 6540 – 6546; b) M. Tabata, Y. Tanaka, Y. Sadahiro, T. Sone, K. Yokota, I. Miura, *Macromolecules* **1997**, *30*, 5200 – 5204.

[18] a) N. Otte, M. Scholten, W. Thiel, *J. Phys. Chem. A* **2007**, *111*, 5751 – 5755; b) W. Weber, W. Thiel, *Theor. Chem. Acc.* **2000**, *103*, 495 – 506; c) E. Millon, J. V. Weber, B. Kubler, J. Theobald, J. F. Muller, *Analysis* **1993**, *21*, 319 – 325; d) G. L. Cui, Z. G. Lan, W. Thiel, *J. Am. Chem. Soc.* **2012**, *134*, 1662 – 1672; e) D. P. Hu, J. Huang, Y. Xie, L. Yue, X. H. Zhuang, Z. G. Lan, *Chem. Phys.* **2015**, *463*, 95 – 105; f) J. B. Schonborn, B. Hartke, *Phys. Chem. Chem. Phys.* **2014**, *16*, 2483 – 2490; g) M. R. Silva-Junior, W. Thiel, *J. Chem. Theory Comput.* **2010**, *6*, 1546 – 1564; h) D. D. Tang, W. H. Fang, L. Shen, G. L. Cui, *Phys. Chem. Chem. Phys.* **2019**, *21*, 17109 – 17117; i) W. Thiel, *MNDO Program*, *version 7.0*, Max-Planck-Institut für Kohlenforschung: Mülheim an der Ruhr, Germany, **2005**.

[19] M. Kasha, *Discuss. Faraday Soc.* **1950**, *9*, 14 – 19.

[20] a) Y. J. Jin, T. Aoki, G. Kwak, *Angew. Chem. Int. Ed.* **2020**, *59*, 1837 – 1844; *Angew. Chem.* **2020**, *132*, 1853 – 1860; b) M. Alzubi, S. Arias, R. Rodríguez, E. Quiñoá, R. Riguera, F. Freire, *Angew. Chem. Int. Ed.* **2019**, *58*, 13365 – 13369; *Angew. Chem.* **2019**, *131*, 13499 – 13503, c) F. Rey-Tarrio, R. Rodríguez, E. Quiñoá, R. Riguera, F. Freire, *Angew. Chem. Int. Ed.* **2021**, *60*, 8095 – 8103; *Angew. Chem.* **2021**, *133*, 8176 – 8184; d) L. Palomo, R. Rodríguez, S. Medina, E. Quiñoá, J. Casado, F. Freire, F. J. Ramírez, *Angew. Chem. Int. Ed.* **2020**, *59*, 9080 – 9087; *Angew. Chem.* **2020**, *132*, 9165 – 9172; e) K. Cobos, R. Rodríguez, E. Quiñoá, R. Riguera, F. Freire, *Angew. Chem. Int. Ed.* **2020**, *59*, 23724 – 23730; *Angew. Chem.* **2020**, *132*, 23932 – 23938; f) B. Fernández, R. Rodríguez, A. Rizzo, E. Quiñoá, R. Riguera, F. Freire, *Angew. Chem. Int. Ed.* **2018**, *57*, 3666 – 3670; *Angew. Chem.* **2018**, *130*, 3728 – 3732; g) S. Arias, R. Rodríguez, E. Quiñoá, R. Riguera, F. Freire, *J. Am. Chem. Soc.* **2018**, *140*, 667 – 674; h) K. Cobos, E. Quiñoá, R. Riguera, F. Freire, *J. Am. Chem. Soc.* **2018**, *140*, 12239 – 12246; i) Z. Fernández, B. Fernández, E. Quiñoá, R. Riguera, F. Freire, *Chem. Sci.* **2020**, *11*, 7182 – 7187; j) B. Nieto-Ortega, R. Rodríguez, S. Medina, E. Quiñoá, R. Riguera, J. Casado, F. Freire, F. J. Ramírez, *J. Phys. Chem. Lett.* **2018**, *9*, 2266 – 2270; k) K. Cobos, R. Rodríguez, O. Domarco, B. Fernández, E. Quiñoá, R. Riguera, F. Freire, *Macromolecules* **2020**, *53*, 3182 – 3193.

[21] L. Arrico, L. Di Bari, F. Zinna, *Chem. Eur. J.* **2021**, *27*, 2920 – 2934.

Manuscript received: June 16, 2021
Revised manuscript received: July 15, 2021
Accepted manuscript online: July 26, 2021
Version of record online: August 31, 2021

 © 2021 Wiley-VCH GmbH